DOI: 10.1002/chem.201001002

Direct Conversion of Commercial Silver Foils into High Aspect Ratio AgBr Nanowires with Enhanced Photocatalytic Properties

Yingpu Bi and Jinhua Ye*[a]

One-dimensional (1D) semiconductor nanostructures, such as nanowires and nanotubes, have recently attracted considerable attention due to their unique electronic and optoelectronic properties, as well as potential applications in fabricating nanoscale devices.[1–5] Over the past decade, semiconductor nanowires of various material systems, including elements (Si, Ge),[6] III–V compounds (GaAs, GaP, InP, InAs),[7] II–VI compounds (ZnS, ZnSe, CdS, CdSe),[8] and oxides (ZnO, MgO, SiO_2),[9] have been successfully fabricated in high yields and uniformity by using diverse techniques. In contrast, the synthesis of silver halide 1D nanostructures, especially silver bromide (AgBr), has lingered far behind. To the best of our knowledge, the synthesized AgBr nanoproducts reported previously mostly possess irregular structures,[10,11] and 1D AgBr nanostructures have been rarely reported until now, especially using templateless methods. However, it is known that AgBr exhibits unique light-sensitive, electrical, and ionic transport properties, which have been widely utilized in photography, electrodes, infrared spectroscopy, radiometry, and heterodyne detection for decades or, in some cases, over a century.[12] Furthermore, it has recently been found that AgBr could also serve as highly stable and active catalysts for various photocatalytic reactions under visible-light irradiation.[13] Thus, the exploration of facile and efficient methods for the large-scale fabrication of high quality 1D AgBr nanostructures may greatly improve their current performance and open up new applications.

Herein, we demonstrate a simple and powerful strategy for the direct conversion of commercial Ag foils into high aspect ratio AgBr nanowires in aqueous Fe^{3+}, Br^-, and polyvinylpyrrolidone (PVP) at room temperature. Moreover, studies of their photocatalytic performance in the decomposition of methylic orange (MO) indicate that these novel AgBr nanowires exhibited excellent catalytic activity under visible-light illumination.

Figure 1A–C and Figure S1 show typical SEM images of the AgBr nanoproducts that were obtained by immersing the commercial Ag foils into an aqueous solution of PVP that contained Fe^{3+} and Br^- ions for 8 h at room temperature, during which the Ag foils serve as both a silver ion source and a substrate for the heteroepitaxial growth of AgBr nanowires. It can be clearly seen from Figure 1A and Figure S1A that large quantities of AgBr nanowires with lengths of up to several tens of micrometers have been synthesized in high yield by this simple replacement process. Figure 1B and Figure S1B–C show the enlarged SEM images of as-synthesized AgBr nanostructures and show

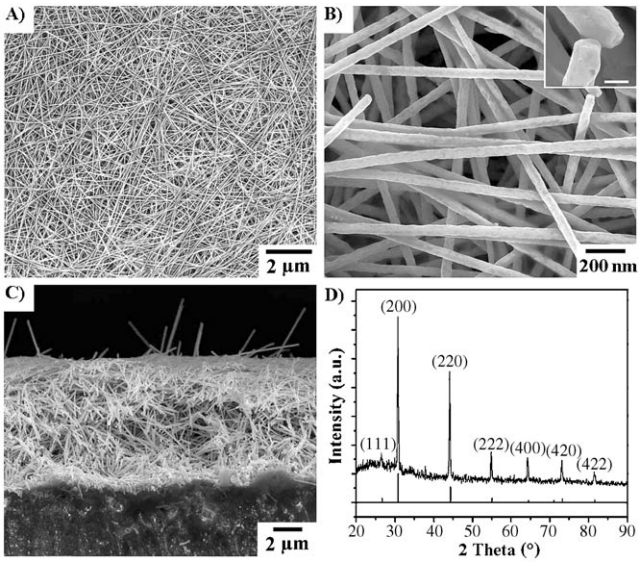

Figure 1. A,B) SEM images of AgBr nanowires on the Ag foil (inset scale bar = 50 nm); C) SEM image of cross-section of the AgBr nanowires on Ag foil; D) XRD pattern of AgBr nanowires.

[a] Y. Bi, J. Ye
International Center for Materials Nanoarchitectonics (MANA) and Photocatalytic Materials Center
National Institute for Materials Science (NIMS)
1-2-1 Sengen, Tsukuba, Ibaraki 305-0047 (Japan)
Fax: (+81) 29-859-2301
E-mail: jinhua.ye@nims.go.jp

Supporting information for this article is available on the WWW under http://dx.doi.org/10.1002/chem.201001002.

that these nanowires possess uniform diameters (≈70 nm) and smooth surfaces (Figure 1B, inset). The cross-section images of the AgBr nanowire/Ag foil products (Figure 1C and Figure S2) suggest that the AgBr layers are composed of dense nanowires with thicknesses of about 10 μm. The X-ray diffraction (XRD) pattern of AgBr nanowires shown in Figure 1D indicates that all peaks of products could be assigned to diffraction from the (111), (200), (220), (222), (400), (420), and (422) planes of the AgBr crystals (PCPDF No.06-0438). Moreover, the EDS results (Figure S3) indicate that except for Cu and Zn in the supports, only Ag and Br were observed in this EDS pattern. Furthermore, it should be noted that the PVP plays a crucial role in determining the morphologies and structures of the AgBr nanoproducts. As shown in Figure S4A, the diameters of the AgBr nanowires were reduced to about 50 nm when the PVP concentration was increased to 200 mM, and no obvious structural change was observed. However, on decreasing the PVP concentration to 100 mM, needle-like AgBr nanowires with large diameters (≈100 nm) were synthesized (Figure S4D). On further decreasing the PVP concentration to 50 mM, the as-synthesized AgBr nanoproducts were composed of rods and particles (Figure S4E). In the absence of PVP, only irregular AgBr particles formed on the Ag foil surfaces (Figure S4G). On the other hand, if PVP was replaced by poly(vinyl alcohol) (PVA), some rod-like nanostructures were obtained, which indicated that the PVA molecule has a similar function to PVP in promoting the formation of 1D AgBr nanostructures (Figure S5A). Moreover, in the presence of cetyltrimethylammonium bromide (CTAB), only porous AgBr nanolayers were formed (Figure S5C). Accordingly, we speculate that the particular adsorption (see Figure S6) and structure induction of PVP may promote the heteroepitaxial growth of AgBr nanowires on the surface of Ag foils and give products with uniform 1D nanostructures.[14]

During the synthesis of AgBr nanowires, the samples were quenched at various time intervals to study their possible growth mechanism. Figure 2 and Figure S7 show typical SEM images of the morphological and structural evolution involved in the growth process of these novel AgBr nanowires. As shown in Figure 2A, the Ag foils possess relatively smooth and clean surfaces prior to the galvanic replacement reactions. However, when the silver foils were dipped into an aqueous PVP solution that contains both Fe^{3+} and Br^- ions, the replacement process between metallic Ag and the Fe^{3+} ions occurred immediately. As shown in Figure 2B, uniform AgBr nanocrystals with octahedron-like structures formed tidily on the surfaces of Ag foils. At longer reaction times, the formed AgBr nanocrystals attached to each other and self-assembled into tower-like nanostructure arrays under the direction of PVP. At $t=2$ h, the length of AgBr nanostructure arrays were increased; at this growth stage the nanoproducts possess flexible structures that grow parallel to the Ag foils (Figure 2D), which may be due to the increase in their length. Furthermore, these AgBr nanostructures gradually transformed into uniform nanowires with high aspect ratios (Figure 2E), which were composed of repeated rectangular AgBr nanocrystals (Figure S8). At $t=$ 6 h, the sharp edges of AgBr nanowires are gradually truncated and transformed into irregular structures (Figure 2F) as a result of their relatively high surface energy. Finally, uniform AgBr nanowires with smooth surfaces (Figure 1B) evolved as a result of the Ostwald ripening process.

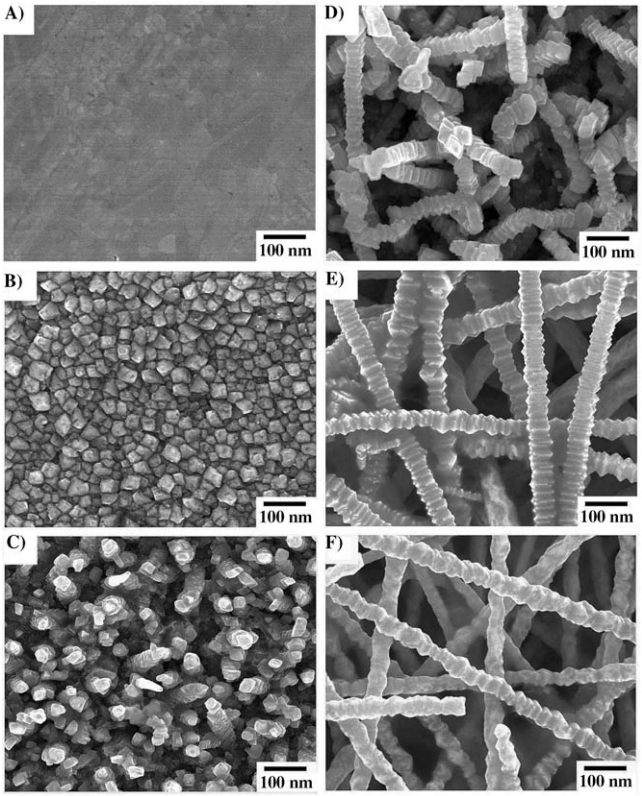

Figure 2. SEM images of AgBr nanowires during growth process at different reaction times: A) 0, B) 0.5, C) 1, D) 2, E) 4, F) 6 h.

Furthermore, the crystalline structure and plasmon absorption of AgBr nanoproducts during the growth process have also been clarified. As shown in Figure 3A, the diffraction peaks of metallic Ag crystals were gradually reduced as the reaction time increased, whereas the peaks of the AgBr crystals were significantly enhanced, which indicates that the lengths and layer thickness of AgBr nanowires greatly increased. Finally, only diffraction peaks of AgBr nanowires were observed due to the relatively thick AgBr nanowire layer (≈10 μm). Moreover, the plasmon absorption spectra of the samples at various growth stages are shown in Figure 3B. Before the galvanic replacement reactions, the Ag foils exhibit a sharp absorption peak at $\lambda=340$ nm and high reflection bands in the range of $\lambda=350$ to 800 nm, which may be due to their smooth and silvery-white surfaces. However, when the growth process of AgBr nanowires has been initiated, the plasmon absorption peaks of metallic Ag crystals markedly reduced, and the absorption peaks of AgBr crystals gradually increased, which is consistent with the XRD results above.[15] Furthermore, except for the metallic Ag and AgBr crystals, no absorption or diffraction peaks

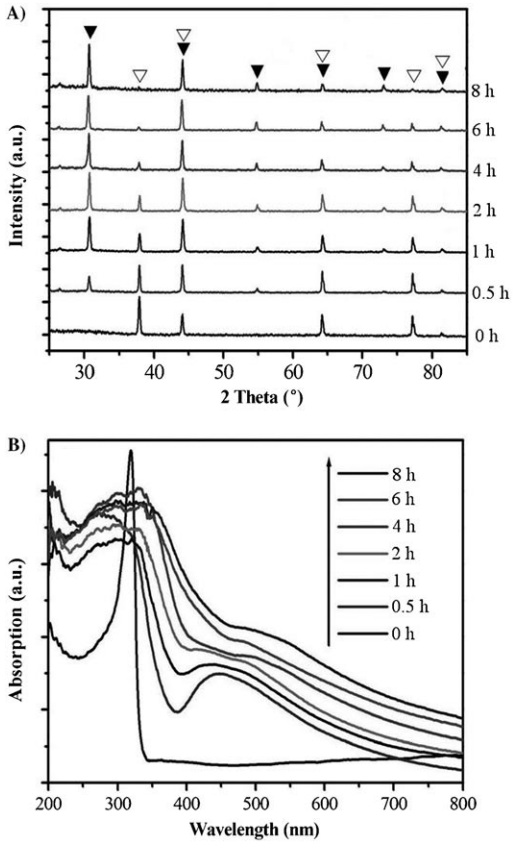

Figure 3. A) XRD patterns (▽: Ag, ▼: AgBr) and B) UV/Vis spectra of AgBr nanowires during the growth process.

corresponding to other impurities were detected during the whole growth process of AgBr nanowires.

Until now, the Ag-engaged galvanic replacement reaction has been widely employed by many groups for preparation of hollow metal nanostructures. It should be noted that these Ag sacrificial templates should possess nanoscale structures and dimensions. Moreover, the redox potential of metal ions, such as the Au^{3+}/Au pair (1.50 V vs. SHE), the Pt^{2+}/Pt pair (1.2 V), and the Pd^{2+}/Pd pair (0.95 V), should be higher than that of Ag^{+}/Ag pair (0.80 V).[16] However, in our synthesis system, the replacement reaction between Fe^{3+} ($E^{\ominus}_{Fe^{3+}/Fe^{2+}} = 0.771$ V) and commercial bulk Ag materials can proceed quite readily at room temperature and AgBr nanowires with uniform diameters and high aspect ratios can be synthesized in large quantities. Herein, we identified a potential replacement mechanism to explain the epitaxial growth process of AgBr nanowires on Ag substrates; the schematic illustration is shown in Scheme 1. In this synthesis system, the Br^{-} ions not only served as a bromide source for the growth of AgBr nanocrystals but also as an activation agent to initiate the replacement reaction. Furthermore, in the presence of Br^{-} ions, the redox potential of Ag species decreased markedly from +0.80 V (Ag^{+}/Ag pair) to +0.007 V (AgBr/Ag pair), which is much lower than that of the Fe^{3+}/Fe^{2+} pair. Therefore, Fe^{3+} ions can directly oxidize the surface Ag atoms of bulk foils into AgBr

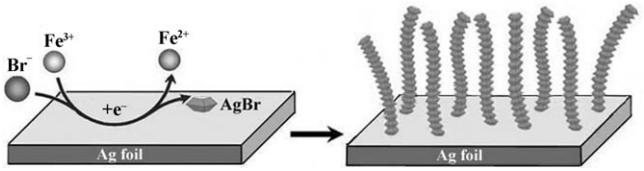

Scheme 1. Schematic illustration of the heteroepitaxial growth process of AgBr nanowires on Ag substrates. Reaction: $Ag + Fe^{3+} + Br^{-} \rightarrow AgBr + Fe^{2+}$; anode reaction: $Ag + Br^{-} \rightarrow AgBr + e^{-}$, $E^{0} = +0.007$ V; cathode reaction: $Fe^{3+} + e^{-} \rightarrow Fe^{2+}$, $E^{0} = +0.771$ V.

nanocrystals. Simultaneously, the PVP molecules in this system were selectively adsorbed onto the various crystal facets of AgBr nanocrystals, which may change their growth rates and induce the oriented attachment of the AgBr nanocrystals into 1D wire-like nanostructures on Ag substrates.

To further confirm the above hypothesis regarding the redox potential functions for AgBr nanowire growth, the shape evolutions of as-synthesized nanoproducts in the presence of other halide ions have also been investigated. As shown in Figure 4A, if NaBr is replaced by NaCl in this process, AgCl nanowires with flexible nanostructures are routinely synthesized. However, it should be noted that the quantities and layer thickness of the obtained AgCl nanowires are lower than that of the AgBr nanowires, which may be due to the low growth rates derived from the redox potential of the AgCl/Ag pair (0.223 V). Furthermore, in the presence of NaI, AgI nanoparticles with large dimensions were synthesized on the surface of Ag foils. Additionally, a novel tower-like AgI structure consisting of an oriented attachment of hexagonal plates has also been obtained (Figure 4B, inset). Furthermore, it can be concluded that the standard potential of the AgI/Ag pair (−0.15 V) is lower

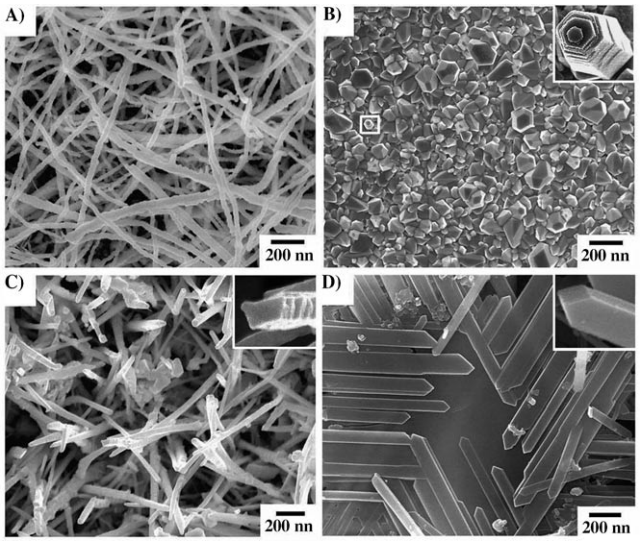

Figure 4. SEM images of the as-synthesized nanoproducts in various systems: A) $Fe(NO_3)_3$ and NaCl, B) $Fe(NO_3)_3$ and NaI, C) AgBr and CuBr, D) AgBr and CuBr prepared in $Cu(NO_3)_2$ and NaBr.

than that of the AgBr/Ag (0.007 V) and AgCl/Ag pairs (0.223 V), which may greatly enhance the replacement rate between Ag and Fe^{3+} and result in a product with irregular structures rather than a wire-like structure. On the other hand, we have also studied the structures of AgBr nanoproducts synthesized by oxidation of other metal ions. The SEM image of AgBr nanoproducts fabricated in the presence of $Cu(NO_3)_2$ and NaBr (Figure 4C) shows that some rod-like nanostructures with rectangular cross-sections are synthesized. Interestingly, when Cu^{2+} ions are reduced to Cu^{+} ions, a novel coproduct, CuBr nanobelts, is also synthesized under the same system (Figure 4D), and the crystal structure and composition can be further confirmed by the XRD and EDS patterns (Figure S9C and D). Furthermore, the above demonstrations suggest that the redox potential of both silver species and metal ions play crucial roles in determining the morphology and structure of AgX ($X = Cl^-$, Br^-, I^-) nanoproducts. More specifically, the generation rates of AgX are strongly dependent on the replacement rates between surface Ag atoms and metal ions, which may control the growth rates of different crystal facets so as to form products with distinct morphologies.

Finally, the photocatalytic behavior of the as-prepared AgBr nanowires were explored for decomposition of MO dye under visible-light irradiation at room temperature.[17] To the best of our knowledge, 1D AgBr nanowires were used as the catalysts for this photocatalytic reaction for the first time. For comparison, the photocatalytic properties of AgBr nanoparticles (see Figure S10), AgCl nanowires, and N-doped TiO_2 were also investigated and the results are shown in Figure 5. It can be clearly seen that all the silver halide photocatalysts exhibit excellent photocatalytic activities for decomposition of MO dye as compared with N-doped TiO_2. Of the silver halides, the AgBr nanowires exhibit the highest photocatalytic activity, and can completely decompose MO dye 2.5 min after visible-light irradiation. Furthermore, spherical AgBr nanoparticles decomposed the MO dye in 6 min, whereas AgCl nanowires required 10 min, which demonstrates that their photocatalytic activities are greatly dependent on the crystal structures and compositions. At present, the photocatalytic mechanism of these AgBr nanowires is not completely understood and a more detailed study is still underway.

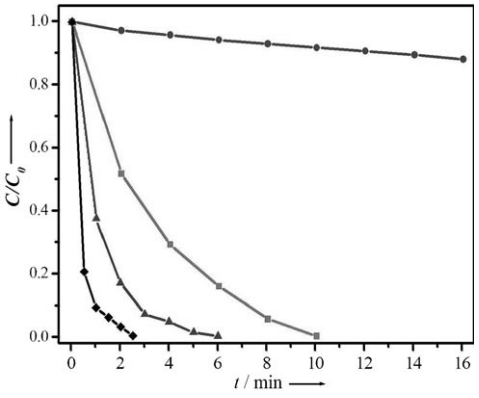

Figure 5. Photocatalytic activity of various catalysts in the decomposition of MO dye under visible-light irradiation at room temperature. ●: N-doped TiO_2, ■: AgCl nanowires, ▲: AgBr nanoparticles, ◆: AgBr nanowires.

In summary, we have demonstrated a facile and efficient replacement process for the large-scale synthesis of uniform and perfect AgBr nanowires from commercial silver foils at room temperature. Moreover, their photocatalytic performance studies indicate that these 1D AgBr nanowires exhibited much higher photocatalytic activity than spherical AgBr nanoparticles and commercial N-doped TiO_2 under visible-light irradiation. Furthermore, we believe that this rational room-temperature synthetic route can also be adapted for the preparation of other semiconductor nanomaterials with special structures, which may have promising photocatalysis, electric, and photoelectric applications.

Experimental Section

AgBr nanowire synthesis: In a typical AgBr nanowires synthesis, the silver foil (4×4 cm) was placed in an aqueous solution of $Fe(NO_3)_3$ (0.5 M), NaBr (0.5 M), and PVP (150 mM). The resulting mixture was maintained at RT until it became yellow in color. The samples intended for morphology and structure analysis were washed with water to remove the $Fe(NO_3)_3$, NaBr, and PVP and dried under atmospheric conditions. The AgBr samples for photocatalytic experiments were obtained by brief sonication of the AgBr naniowire/Ag foils without breaking the AgBr nanowires. For comparison, spherical AgBr nanoparticles were also synthesized by using conventional precipitation methods with surfactant (PVP).

Photocatalytic reactions: In all catalytic activity of experiments, the samples (0.1 g) were put into a solution of MO dye (100 mL, 40 mg L^{-1}), which was then irradiated with a 300 W Xe arc lamp equipped with an ultraviolet cutoff filter ($\lambda \geq 420$ nm). The degradation of MO dye was monitored by using UV/Vis spectroscopy (UV-2500PC, Shimadzu). Before the spectroscopy measurement, these nanowire catalysts were removed from the photocatalytic reaction systems by a dialyzer.

Characterization: SEM and FE-SEM images were taken by using a field-emission scanning electron microscope (JSM-6701F, JEOL) operated at an accelerating voltage of 5 kV. The X-ray diffraction spectra (XRD) measurements were performed on a Philips X'pert MPD instrument by using $Cu_{K\alpha}$ radiation (50 kV). The XRD patterns were recorded from 10 to 90° with a scanning rate of 0.067° s^{-1}. The infrared spectra were obtained by using a Fourier transform infrared (FTIR) spectrometer (Shimadzu IRprestige-21). UV/Vis absorption spectra were taken at room temperature by using a UV-2550 (Shimadzu) spectrometer.

Acknowledgements

This work was partially supported by the World Premier International Research Center Initiative on Materials Nanoarchitectonics, MEXT, and JST-MOST Strategic Japanese–Chinese Cooperative Programme, Japan.

Keywords: bromine · nanostructures · photochemistry · replacement reaction · silver

[1] J. V. Barth, G. Costantini, K. Kern, *Nature* **2005**, *437*, 671.
[2] H. J. Fan, P. Werner, M. Zacharias, *Small* **2006**, *2*, 700.

[3] X. Duan, Y. Huang, Y. Cui, J. Wang, C. M. Lieber, *Nature* **2001**, *409*, 66.
[4] W. Lu, C. M. Lieber, *Nat. Mater.* **2007**, *6*, 841.
[5] Y. Wu, P. Yang, *J. Am. Chem. Soc.* **2002**, *124*, 3136.
[6] a) L. Schubert, P. Werner, N. D. Zakharov, G. Gerth, F. M. Kolb, L. Long, U. Gösele, T. Y. Tan, *Appl. Phys. Lett.* **2004**, *84*, 4968; b) A. I. Hochbaum, R. Fan, R. He, P. Yang, *Nano Lett.* **2005**, *5*, 457.
[7] a) M. T. Björk, B. J. Ohlsson, T. Sass, A. I. Persson, C. Thelander, M. H. Magnusson, K. Deppert, L. R. Wallenberg, L. Samuelson, *Nano Lett.* **2002**, *2*, 87; b) H. Yu, W. E. Buhro, *Adv. Mater.* **2003**, ***15***, 416; c) Q. Xiong, J. Wang, P. C. Eklund, *Nano Lett.* **2006**, *6*, 2736.
[8] C. J. Barrelet, Y. Wu, D. C. Bell, C. M. Lieber, *J. Am. Chem. Soc.* **2003**, *125*, 11498.
[9] M. H. Huang, S. Mao, H. Feick, H. Yan, Y. Wu, H. Kind, E. Weber, R. Russo, P. Yang, *Science* **2001**, *292*, 1897.
[10] S. Liu, J. Yue, A. Gedanken, *Adv. Mater.* **2001**, *13*, 656.
[11] I. V. Rubtsov, K. Ebina, F. Satou, J. Oh, S. Kumazaki, T. Suzumoto, T. Tani, K. Yoshihara, *J. Phys. Chem. A* **2002**, *106*, 2795.
[12] a) B. Trösken, F. Willig, K. Schwarzburg, A. Ehret, M. Spitler, *Adv. Mater.* **1995**, *7*, 448; b) I. Sekerka, J. F. Lechner, *Anal. Lett.* **1976**, *9*, 1099; c) T. W. Richards, E. P. Bartlett, *J. Am. Chem. Soc.* **1915**, *37*, 470.
[13] a) M. R. Elahifard, S. Rahimnejad, S. Haghighi, M. R. Gholami, *J. Am. Chem. Soc.* **2007**, *129*, 9552; b) C. Hu, Y. Lan, J. Qu, X. Hu, A. Wang, *J. Phys. Chem. B* **2006**, *110*, 4066.
[14] a) Z. Zhang, B. Zhao, L. Hu, *J. Solid State Chem.* **1996**, *121*, 105; b) J. Zhang, H. Liu, Z. Wang, N. Ming, Z. Li, A. S. Biris, *Adv. Funct. Mater.* **2007**, *17*, 3897.
[15] a) P. Wang, B. B. Huang, X. Y. Zhang, X. Y. Qin, H. Jin, Y. Dai, Z. Y. Wang, J. Y. Wei, J. Zhan, S. Y. Wang, J. P. Wang, M.-H. Whangbo, *Chem. Eur. J.* **2009**, *15*, 1821; b) P. Wang, B. Huang, Z. Lou, X. Zhang, X. Qin, Y. Dai, Z. Zheng, X. Wang, *Chem. Eur. J.* **2010**, *16*, 538.
[16] a) X. Lu, L. Au, J. McLellan, Z. Y. Li, M. Marquez, Y. Xia, *Nano Lett.* **2007**, *7*, 1764; b) J. Chen, B. Wiley, J. McLellan, Y. Xiong, Z. Y. Li, Y. Xia, *Nano Lett.* **2005**, *5*, 2058; c) Y. Sun, Y. Xia, *J. Am. Chem. Soc.* **2004**, *126*, 3892; d) Y. Sun, B. Wiley, Z. Y. Li, Y. Xia, *J. Am. Chem. Soc.* **2004**, *126*, 9399; e) D. Zhao, B. Yan, B. Xu, *Electrochem. Commun.* **2008**, *10*, 884; f) Y. Bi, J. Ye, *Chem. Commun.* **2010**, *46*, 1532.
[17] a) P. Wang, B. Huang, X. Qin, X. Zhang, Y. Dai, J. Wei, M. Whangbo, *Angew. Chem.* **2008**, *120*, 8049; *Angew. Chem. Int. Ed.* **2008**, *47*, 7931; b) Y. Bi, J. Ye, *Chem. Commun.* **2009**, 6551.

Received: April 19, 2010
Published online: July 23, 2010

